JOURNAL OF APPLIED ELECTROCHEMISTRY 18 (1988) 657–655

Double channel electrodes and the measurement of heterogeneous reaction rates at the solid–liquid interface

RICHARD G. COMPTON, GEOFFREY M. STEARN, PATRICK R. UNWIN, ANTHONY J. BARWISE

Physical Chemistry Laboratory, Oxford University, South Parks Road, Oxford OX1 3QZ, UK

Received 20 January 1988

The theory of collection efficiency measurements (under steady-state conditions) at double channel electrodes is extended to include the case where the species generated at the upstream electrode undergoes a heterogeneous reaction on the surface of the gap between the two electrodes. The problem is treated numerically using the Backwards Implicit method, which allows the collection efficiency to be related to the corresponding value of the rate constant for the heterogeneous process for chosen double electrode geometries and solution flow rates. The use of the technique is illustrated with experiments in which bromine, generated at the upstream electrode by the oxidation of bromide ions (in 0.5 M sulphuric acid), reacts with a cloth dyed with Direct Red 80, and is subsequently collected at the downstream electrode through transport-controlled reduction to bromide. Good agreement is found between theory and experiment.

1. Introduction

Hydrodynamic double electrodes – first introduced by Frumkin and Nekrasov [1] in the form of the rotating ring–disc electrode (RRDE), and later in channel form by Gerischer *et al.* [2] – are unique electrode systems with which electrode reaction mechanisms may be studied. These hydrodynamic electrodes allow the intermediates and products of reactions on an upstream (generator) electrode to be analysed and characterized amperometrically after transport to a downstream detector electrode, as illustrated in Fig. 1. In particular, when the detector electrode is held at a potential at which the destruction of species generated at the upstream electrode is diffusion controlled, kinetic and mechanistic information is available from 'collection efficiency' (N) measurements:

$$N = \frac{\text{current at downstream (detector) electrode}}{\text{current at upstream (generator) electrode}} = \frac{I_{\text{det}}}{I_{\text{gen}}} \quad (1)$$

In the case of the double channel electrode (DCE), theory has been presented for the cases where the electrogenerated intermediate is either stable [2–4] or else decays via first-order kinetics in solution [5].

Whilst the double electrode technique has found widespread application in the investigation of the (homogeneous) solution kinetics of electrogenerated species [6, 7], the possibility of employing the RRDE or the DCE to investigate heterogeneous processes involving such species has hitherto been neglected. It is the aim of this paper to illustrate how the DCE may be modified to facilitate the study of heterogeneous reaction rates involving non-conducting substrates. In this context the upstream electrode is used to generate the reactant from an unreactive precursor contained in the flowing solution. After passing over the substrate under investigation, located in the gap between the upstream and downstream electrodes, the reactant is detected amperometrically at the latter electrode. The measured collection efficiency allows the deduction of the heterogeneous rate constant of the process in question – the faster this reaction, the smaller the observed collection efficiency for a given flow rate and generator electrode–gap–detector electrode geometry.

The mass-transport equations pertaining to this problem are solved using the Backwards Implicit (numerical) method, which has previously been successfully applied in the solution of a number of channel electrode problems, involving a diversity of boundary conditions [8–12]. Since in this appoach the convective–diffusion equation is solved with the full parabolic velocity profile describing the flowing solution under fully-developed laminar conditions (*vide infra*), the theoretical results are applicable to a wide range of electrode–gap geometries. In contrast, an analytical treatment of this problem, employing the Lévêque approximation [4, 5], would necessarily impose severe restrictions on the range of electrode–gap geometries which could be employed practically, thus greatly reducing the applicability of the experiment.

The method is illustrated with reference to experiments in which aqueous bromine, generated by the oxidation of bromide ions at an upstream electrode, reacts with a cotton cloth dyed with Direct Red 80, and is subsequently detected at an electrode immediately downstream, through transport-controlled reduction to bromide. The results of this model system are found to be in good agreement with theory, and show

0021-891X/88 $03.00 + .12

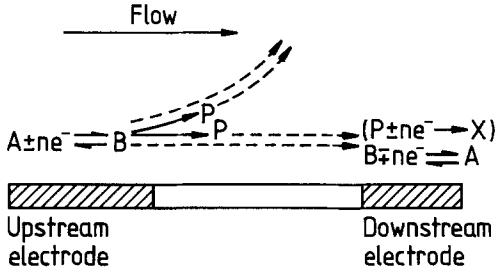

Fig. 1. Principle behind hydrodynamic double electrode operation under steady-state conditions. A proportion of the species B, generated at the upstream electrode, is lost before collection at the detector electrode, via diffusion, reaction in solution or reaction at the interface between the two electrodes. The collection efficiency, N, provides information about these processes. Where the reaction product, P is electroactive, it too may be detected amperometrically.

quantitative comparison with a previous investigation which employed an independent experimental method [13]. The DCE technique is therefore recommended for the evaluation of rate constants of solid/liquid interfacial processes, in general, when the solution component can be generated and detected amperometrically.

2. Theory

The coordinate system adopted for the double electrode flow cell is depicted in Fig. 2. The hydrodynamics of solution flow in cells of this geometry is well documented [14–16] and the general convective–diffusive behaviour of a solution species M is described by:

$$\frac{\partial[\mathrm{M}]}{\partial t} = D_{\mathrm{M}}\nabla^2[\mathrm{M}] - v_x\frac{\partial[\mathrm{M}]}{\partial x} - v_y\frac{\partial[\mathrm{M}]}{\partial y} - v_z\frac{\partial[\mathrm{M}]}{\partial z} \tag{2}$$

where D_{M} is the diffusion coefficient and [M] the concentration of M. v_x, v_y and v_z are solution velocities in the respective Cartesian directions.

We consider conditions of laminar flow [7] in the x-direction; v_y and v_z are zero. It has been shown [16, 17] that for cells of the dimensions employed in practical experiments ($b \ll d$) and with convenient flow rates ($10^{-4}\,\mathrm{cm^3\,s^{-1}} < V_{\mathrm{f}} < 10^{-1}\,\mathrm{cm^3\,s^{-1}}$) that $\nabla^2[\mathrm{M}] \doteq \partial^2[\mathrm{M}]/\partial y^2$ is a good approximation, and that v_x is given by

$$v_x = \left(\frac{6V_{\mathrm{f}}}{bd}\right)\left(\frac{y}{b}\right)\left(1 - \frac{y}{b}\right) \tag{3}$$

Thus, under steady-state conditions, Equation 2 may be written as

$$D_{\mathrm{M}}\frac{\partial^2[\mathrm{M}]}{\partial y^2} - \left(\frac{6V_{\mathrm{f}}}{bd}\right)\left(\frac{y}{b}\right)\left(1 - \frac{y}{b}\right)\frac{\partial[\mathrm{M}]}{\partial x} = 0 \tag{4}$$

In the double electrode experiment described above, a reaction at the upstream electrode converts species A to B, i.e.

$$\mathrm{A} \pm ne^- \rightleftharpoons \mathrm{B} \tag{5}$$

If the electrodes are held at potentials such that the above process is transport limited at the upstream electrode and the reverse process is transport limited at the downstream electrode then the following boundary conditions apply:

upstream ($0 < x < x_1$), $y = 0$:

$$[\mathrm{A}] = 0,\ D_{\mathrm{B}}\frac{\partial[\mathrm{B}]}{\partial y} = -D_{\mathrm{A}}\frac{\partial[\mathrm{A}]}{\partial y} \tag{6}$$

downstream ($x_2 < x < x_3$), $y = 0$:

$$D_{\mathrm{A}}\frac{\partial[\mathrm{A}]}{\partial y} = -D_{\mathrm{B}}\frac{\partial[\mathrm{B}]}{\partial y},\ [\mathrm{B}] = 0 \tag{7}$$

If species B undergoes a heterogeneous reaction at the cell wall between the electrodes with rate constant k (in $\mathrm{cm\,s^{-1}}$), then:

$$D_{\mathrm{B}}\left.\frac{\partial[\mathrm{B}]}{\partial y}\right|_{y=0} = k\,[\mathrm{B}] \tag{8}$$

and thus the boundary condition

$$(x_2 < x < x_1),\ y = 0:\ \frac{\partial[\mathrm{A}]}{\partial y} = 0,\ \frac{\partial[\mathrm{B}]}{\partial y} = \frac{k[\mathrm{B}]}{D_{\mathrm{B}}} \tag{9}$$

follows. The remaining boundary conditions are:

$$x = 0:\quad [\mathrm{A}] = [\mathrm{A}]_\infty,\ [\mathrm{B}] = 0 \tag{10}$$

$$y = b:\quad \frac{\partial[\mathrm{A}]}{\partial y} = \frac{\partial[\mathrm{B}]}{\partial y} = 0 \tag{11}$$

where $[\mathrm{A}]_\infty$ is the bulk concentration of species A upstream of the cell.

The collection efficiency, N is given by

$$N = \frac{i_{\mathrm{det}}}{i_{\mathrm{gen}}} = \left\{D_{\mathrm{B}}\int_{x_2}^{x_3}\left(\frac{\partial[\mathrm{B}]}{\partial y}\right)_{y=0}\mathrm{d}x\right\}\Big/\left\{D_{\mathrm{A}}\int_0^{x_1}\left(\frac{\partial[\mathrm{A}]}{\partial y}\right)_{y=0}\mathrm{d}x\right\} \tag{12}$$

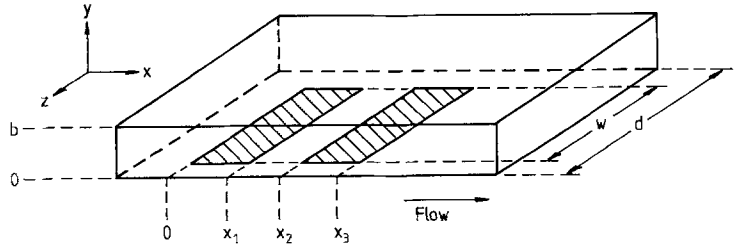

Fig. 2. Double channel electrode geometry.

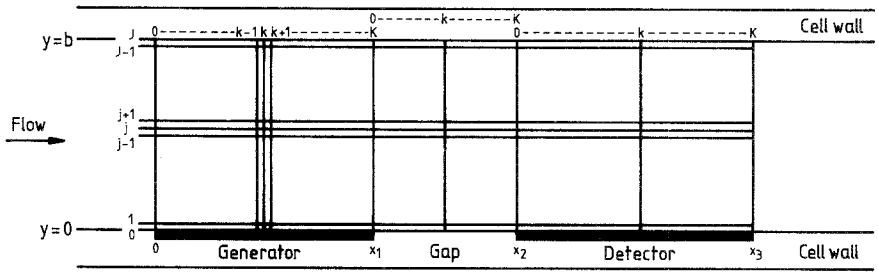

Fig. 3. Two-dimensional (x–y plane) finite difference grid for the numerical solution of collection efficiencies at the double channel electrode.

Convective-diffusion Equations 2 for A and B have been solved analytically by Braun [3] and Matsuda [4] to yield collection efficiencies as a function of electrode geometry. This analytical approach involved the further simplification of linearizing the velocity profile, v_x:

$$V_x = \left(\frac{6V_f}{bd}\right)\left(\frac{y}{b}\right)\left(1 - \frac{y}{b}\right) \approx \left(\frac{6V_f}{bd}\right)\left(\frac{y}{b}\right) \qquad (13)$$

This is the Lévêque approximation [18] and is clearly valid in the region where $y \ll b$, or equivalently where [14]:

$$D\,dx_1 \ll V_f\,b/2 \qquad (14)$$

In order to produce results of a more general nature, we have retained the full parabolic velocity profile, as described by Equation 3, by adoption of a numerical method. The Backward Implicit finite difference method, identified by Anderson [9] as that most suited to channel electrode problems, was chosen.

For the purposes of the calculation, the cell is divided into three regions ($0 < x < x_1$; $x_1 < x < x_2$; $x_2 < x < x_3$) and the Backward Implicit method applied to each region in turn. For each region the numerical solution involves covering the xy plane with a finite difference grid of dimension $J \times K$ (Fig. 3). Values of J and K are chosen such that the numerical solution converges to the required accuracy. In the calculations described below, $J = 500$ and $K = 500$ were used in each region. Clearly for compatibility, J must be the same throughout the channel. Increments in the x direction are Δx and in the y direction Δy where

$$y_j = j\Delta y \quad (j = 0, 1. \ldots J), \quad \Delta y = b/J$$

$$x_k = k\Delta x \quad (k = 0, 1. \ldots K), \quad \Delta x = x^*/K$$

x^* is x_1, $x_2 - x_1$ or $x_3 - x_2$ in the various regions. Derivatives are approximated to

$$\frac{\partial g^M}{\partial x} = \frac{g^M_{j,k+1} - g^M_{j,k}}{\Delta x}, \quad \frac{\partial g^M}{\partial y} = \frac{g^M_{j+1,k+1} - g^M_{j,k+1}}{\Delta y} \qquad (15)$$

and

$$\frac{\partial^2 g^M}{\partial y^2} = \frac{g^M_{j-1,k+1} - 2g^M_{j,k+1} + g^M_{j+1,k+1}}{(\Delta y)^2} \qquad (16)$$

where g^M are normalized concentrations

$$g^A = [A]/[A]_\infty, \; g^B = [B]/[A]_\infty \qquad (17)$$

Substituting these expressions into Equation 4 gives the following $J - 1$ simultaneous equations:

$$\lambda^M_j\,(g^M_{k+1,k+1} - 2g^M_{j,k+1} + g^M_{j+1,k+1}) = g^M_{j,k+1} - g^M_{j,k}, \quad j = 1, 2. \ldots J - 1 \qquad (18)$$

where

$$\lambda^M_j = \frac{D_M \Delta x b^3 d}{6V_f j\,(\Delta y)^3\,(b - j\Delta y)} \qquad (19)$$

or

$$g^M_{j,k} = -\lambda^M_j g^M_{j-1,k+1} + (2\lambda^M_j + 1)\,g^M_{j,k+1} - \lambda^M_j g^M_{j+1,k+1} \qquad (20)$$

Thus the vector $\{g^M_{k+1}\}$ is related to $\{g^M_k\}$ by a set of $J - 1$ simultaneous equations. Application of the boundary conditions 6, 7, 9 and 11 eliminates the terms in $g^M_{0,k+1}$ and in $g^M_{J,k+1}$ and permits the expression of the equations as a $(J - 1) \times (J - 1)$ matrix equation.

The boundary conditions 6, 7, 9 and 11 become

$y = 0, 0 < x < x_1$:

$$g^A_{0,k+1} = 0, \; g^B_{0,k+1} = g^B_{1,k+1} + \frac{D_A}{D_B} g^A_{1,k+1} \qquad (21)$$

$y = 0, x_2 < x < x_3$:

$$g^A_{0,k+1} = g^A_{1,k+1} + \frac{D_B}{D_A} g^B_{1,k+1}, \; g^B_{0,k+1} = 0 \qquad (22)$$

$y = 0, x_1 < x < x_2$:

$$g^A_{0,k-1} = g^A_{1,k+1}, \; g^B_{0,k+1} = \frac{g^B_{1,k+1}}{1 + k\Delta y/D_B} \qquad (23)$$

$y = b, 0 < x < x_3$:

$$g^A_{J,k+1} = g^A_{J-1,k+1}, \; g^B_{J,k+1} = g^B_{J-1,k+1} \qquad (24)$$

The equations may then be written as:

$$\begin{bmatrix} d_1 \\ d_2 \\ \vdots \\ d_j \\ \vdots \\ d_{J-2} \\ d_{J-1} \end{bmatrix} = \begin{bmatrix} b_1 & c_1 & 0 & & & \\ a_2 & b_2 & c_2 & 0 & & \\ \cdot & \cdot & \cdot & & & \\ 0 & a_j & b_j & c_j & 0 & \\ & & \cdot & \cdot & \cdot & \\ & & a_{J-2} & b_{J-2} & c_{J-2} & \\ & & 0 & a_{J-1} & b_{J-1} & \end{bmatrix} \begin{bmatrix} u_1 \\ u_2 \\ \vdots \\ u_j \\ \vdots \\ u_{J-2} \\ u_{J-1} \end{bmatrix}$$

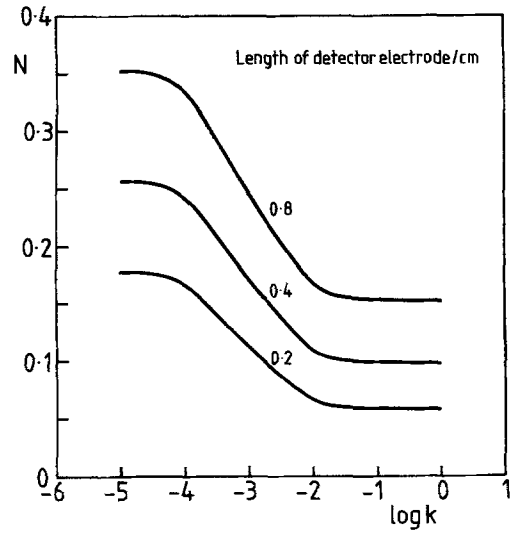

Fig. 4. The effect on N–k behaviour of changing the length of the detector electrode. The data relates to channel electrode/flow cell parameters of $x_1 = 0.2$, $x_2 = 0.6$, $x_3 = 0.8$, 1.0 and 1.4 cm, $b = 0.1$ cm, $d = 0.6$ cm, $w = 0.4$ cm, $V_f = 10^{-2}$ cm^3 s^{-1}, $D = 10^{-5}$ cm^2 s^{-1}.

where a_j, b_j, c_j, d_j and u_j, have the following values in the various regions for species A and B.

In all regions:

$$u_j^M = g_{j,k+1}^M \quad j = 1, 2 \ldots J-1$$
$$a_j^M = -\lambda_j^M \quad j = 2, 3 \ldots J-1$$
$$c_j^M = -\lambda_j^M \quad j = 1, 2 \ldots J-2$$
$$b_j^M = 2\lambda_j^M + 1 \quad j = 2, 3 \ldots J-2$$
$$d_j^M = g_{j,k}^M \quad j = 2, 3 \ldots J-1$$
$$b_{J-1}^M = \lambda_{J-1}^M + 1$$

M refers to both A and B

$$0 < x < x_1: b_1^A = 2\lambda_1^A + 1, \; b_1^B = \lambda_1^B + 1$$
$$d_1^A = g_{1,k}^A,$$
$$d_1^B = g_{1,k}^B + g_{1,k+1}^A \lambda_1^B D_A/D_B$$

$$x_1 < x < x_2: b_1^A = \lambda_1^A + 1,$$
$$b_1^B = 1 + \lambda_1^B[2 - 1/(1 + k\Delta y/D_B)]$$
$$d_1^A = g_{1,k}^A, \; d_1^B = g_{1,k}^B$$

$$x_2 < x < x_3: b_1^A = \lambda_1^A + 1, \; b_1^B = 2\lambda_1^B + 1$$
$$d_1^A = g_{1,k}^A + g_{1,k+1}^B \lambda_1^A D_B/D_A,$$
$$d_1^B = g_{1,k}^B$$

The matrix, being of tridiagonal form may be solved by a recursion relationship known as the Thomas algorithm [19] to give $\{g_{k+1}^M\}$ from $\{g_k^M\}$. Thus, knowing the vector $\{g_0^M\}$ from the boundary condition 10, $\{g_1^M\}$ is obtained an so on up to $\{g_K^M\}$. Then a new grid is set up for the second region ($x_1 < x < x_2$), the computed $\{g_K^M\}$ becoming the new $\{g_0^M\}$. The above procedure is repeated for the second and third regions so that $g_{j,k}^A$ and $g_{j,k}^B$ are known for all j and k in each grid.

The collection efficiency N is then determined by

$$N = \left(\frac{D_B}{D_A}\right)\left\{\sum_{x_2}^{x_3} g_{1,k}^B\right\} \Big/ \left\{\sum_{0}^{x} g_{1,k}^A\right\} \qquad (25)$$

In each summation k is summed from 1 to K.

The computation was carried out via a Fortran program excecuted on a Norsk Data ND540 mainframe computer. 'Working curves' of the collection efficiency, N vs k, the heterogeneous rate constant for the 'gap reaction', were generated for specified DCE geometries and flow rates. Typical working curves are shown in Figs 4–6, illustrating the effect of independently varying the length of the gap, detector electrode and solution flow rate, whilst keeping the other DCE/cell parameters constant. As expected, maximum sensitivity in the measurement of k, via the technique, is achieved by maximizing the length of the detector electrode. This is shown in Fig. 4. Figures 5a and 5b point to an optimal value for the length of the gap, for fixed detector and generator electrode lengths and flow rate. In the example given, where $x_1 = 0.2$, $x_3 - x_2 = 0.4$ cm, $V_f = 10^{-2}$ cm^3 s^{-1}, $D = 10^{-5}$ cm^2 s^{-1}, $d = 0.6$ cm and $b = 0.1$ cm, this is obtained with a gap length of around 0.2 cm. Smaller or larger gap lengths result in a diminution in sensitivity. In the former case, this arises since an insufficient length of substrate is exposed to the reactant to cause significant depletion before detection downstream, whilst in the latter, a significant proportion of the electrogenerated reactant is lost to the bulk solution in its transit downstream. It is apparent from Fig. 6 that the range of rate constants to which the technique may be applied depends critically upon the range of flow rates available. With the parameters used to generate the data in Fig. 6 ($x_1 = 0.2$, $x_2 = 0.3$, $x_3 = 0.7$ cm, $V_f = 10^{-3}$, 10^{-2}, 10^{-1} and 1 cm^3 s^{-1}, $D = 10^{-5}$ cm^2 s^{-1}, $d = 0.6$ cm and $b = 0.1$ cm), heterogeneous rate constants in the range 10^{-1}–10^{-5} cm s^{-1} may be measured. The general observation to be made is that slower flow rates favour the measurement of slow rate constants.

3. Experimental details

3.1. *The flow cell and flow system*

The flow cell and flow system have previously been described [13, 15], and so only a brief description will be given here. Experiments were carried out using the cell shown in Fig. 7, which was fabricated in Perspex. The channel is 40 mm long, 6 mm wide and approximately 1 mm deep. A precise value for the latter parameter was found from the slope of a Levich plot (transport-limited current vs (flow rate $^{1/3}$) [20], obtained from an electroactive species of known diffusion coefficient.

A cover plate bore the substrate – in this case a piece of cotton cloth – onto which were cemented to the electrodes. The electrodes consisted of strips cut from platinum foil, 0.025 mm thick (99.95%, Goodfellows, Cambridge, UK).

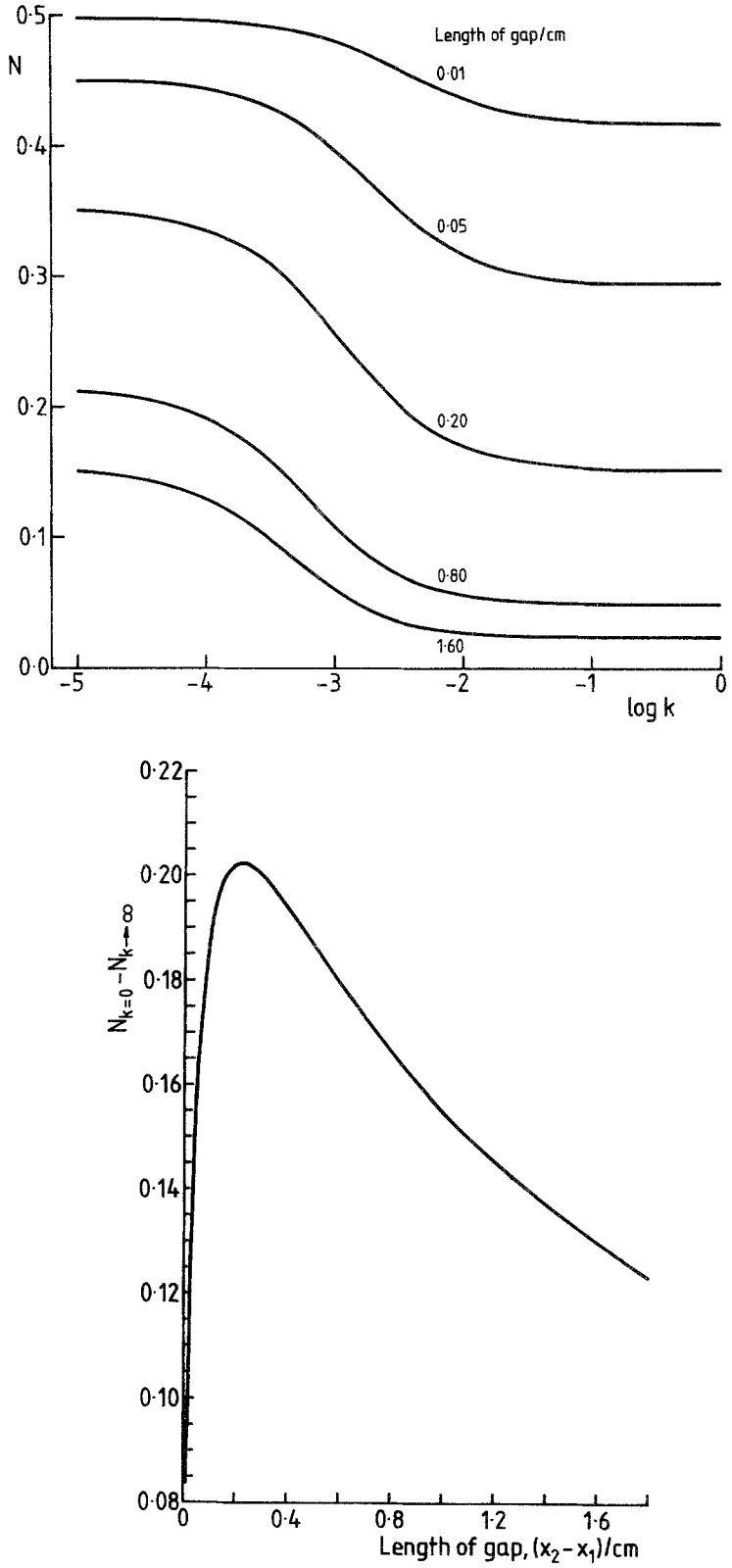

Fig. 5. (a) N–k behaviour for various gap lengths $(x_2 - x_1)$. Parameters employed in the calculations were $x_1 = 0.2$ cm, $(x_3 - x_2) = 0.4$ cm, $b = 0.1$ cm, $d = 0.6$ cm, $w = 0.4$ cm, $V_f = 10^{-2}$ cm^3 s^{-1}, $D = 10^{-5}$ cm^2 s^{-1}. (b) The effect on sensitivity (defined as being the difference in shielding factors for the case when there is no heterogeneous reaction in the gap to that when the reaction is diffusion controlled, i.e. $N_{k=0} - N_{k\to\infty}$) of varying the length of the gap for constant generator and detector electrode lengths and solution flow rate. Parameters employed were those used to generate the data in (a).

The upstream electrode was located 3–4 mm downstream of the upstream edge of the cloth, and the upstream region of the substrate was masked from the solution with thin PTFE tape, as shown in Fig. 7. The edges of the substrate and electrodes were treated in the same manner, as illustrated, so that the width of the exposed substrate and electrodes was approximately 4 mm. This arrangement ensured that flow over the reactive interface was of a plug nature with respect to the z direction; edge effects (in which v_x deviates from the expression given in Equation 3), occur over distance $\sim b/2$ [15]. In general, the lengths

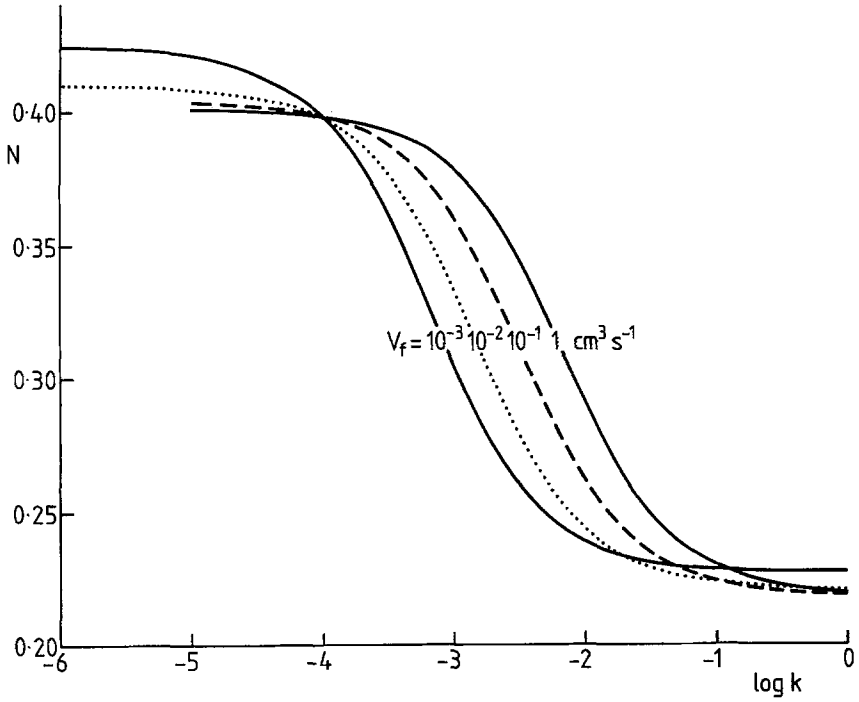

Fig. 6. N–k behaviour as a function of flow rate, for $x_1 = 0.2$, $x_2 = 0.3$, $x_3 = 0.7$ cm, $b = 0.1$ cm, $d = 0.6$ cm, $w = 0.4$ cm and $D = 10^{-5}\,cm^2 s^{-1}$.

of the upstream and downstream electrodes were of the order of 2 and 4 mm, respectively, with a gap of ~ 1 mm.

The channel was formed by mating the channel unit and cover plate through the application of mechanical pressure, the O-ring aroung the channel acting as a seal.

The flow system, into which the cell was plumbed, consisted of a glass reservoir, and several metres of 1.5 mm bore PTFE tubing (Anachem, Luton, UK), jacketed with an Argon-purged tube to prevent the ingress of oxygen. The standard 'three-electrode' configuration was achieved by locating a platinum gauze counter electrode immediately downstream of the cell and incorporating a chloridized silver wire into the upstream duct of the channel, to act as a pseudo-reference electrode.

Connections between the PTFE tubing, the cell and the counter electrode were formed with silicone rubber tubing. Deoxygenated electrolyte was gravity fed from the reservoir via one of several calibrated glass capillaries, which gave a total flow rate range of 10^{-4}–$3 \times 10^{-1}\ cm^3\ s^{-1}$. Adjustment of the rate of flow with each capillary was achieved by varying the height between the reservoir and the tip of the capillary, where the electrolyte ran to waste.

Electrical contact to the two working electrodes was facilitated by extending the foils beyond the edge of the coverplate as illustrated in Fig. 7. Locating the cell and about 1 m of the preceeding tubing within an air thermostat allowed temperature control to 25 ± 0.1°C.

3.2. *Materials*

Solution were made up using triply distilled deionized water (resistivity $> 10^7\ \Omega$cm). Ferricyanide solutions constituted approximately 5×10^{-3} M potassium ferricyanide in 0.1 M sodium hydroxide and 1 M potassium

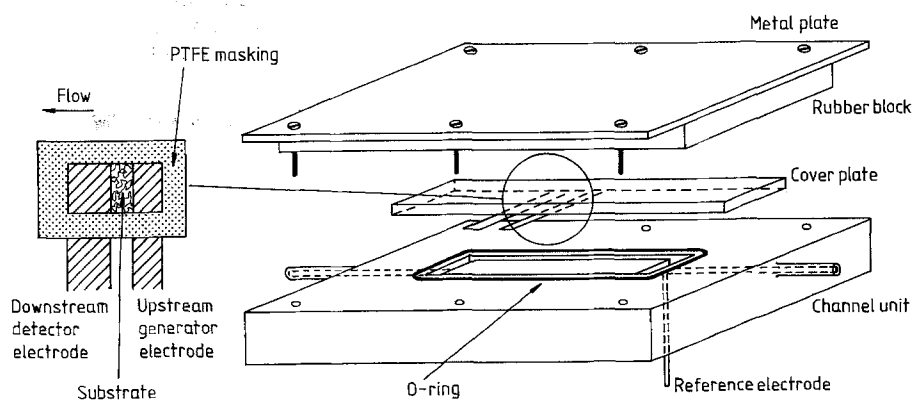

Fig. 7. Double channel electrode cell.

chloride to serve as background electrolyte. Bromide solutions were approximately 10^{-3} M in sodium bromide, 0.5 M sulphuric acid acting as background electrolyte. Reagents were BDH AnalaR grade. Cotton cloth, stained with the dye Direct Red 80, was provided by Unilever Research (Merseyside, UK).

3.3. *Techniques*

Collection efficiencies were measured by changing the generator electrode potentials through such a range of values as to change the reaction of interest from being essentially undriven to a state of almost transport control ($Br^- \rightarrow Br_2$, +0.70 to +1.10 V; $Fe(CN)_6^{3-} \rightarrow Fe(CN)_6^{4-}$, +0.4 to 0.0 V versus Ag/AgCl-reference) whilst maintaining the detector electrode at a potential so as to drive the reverse reaction at a transport-controlled rate. The potential change was effected by small stepwise increments (5–10 mV). After due time for true steady-state conditions to be established, the currents at both electrodes were measured directly. Plots of I_{det} vs I_{gen} were found to be closely linear and the gradient afforded a measure of N.

4. Results and discussion

Preliminary experiments concerning the reduction of ferricyanide over a wide range of flow rates at a short (~2 mm) single platinum electrode were conducted to verify that the flow cell hydrodynamics were as suggested above. These have been reported elsewhere [13] where it was concluded that this indeed was the case, transport-limited currents being found to be (flow rate)$^{1/3}$-dependent, as predicted by the Levich equation [20]. Subsequent experiments were performed in order to demonstrate the validity, or otherwise, of the theory developed above for the case when the reactant generated on the upstream electrode was engaged in no heterogeneous (or homogeneous) reaction during transit to the detector electrode. To this end, the $Fe(CN)_6^{4-/3-}$ system in aqueous solution at pH 13 (0.1 M NaOH) was studied at a platinum DCE. Ferrocyanide was electrogenerated from Ferricyanide under steady-state conditions at the upstream electrode:

upstream electrode: $Fe(CN)_6^{3-} + e^- \longrightarrow Fe(CN)_6^{4-}$

whilst the downstream electrode was held at a potential such that incoming ferrocyanide ions were oxidized to ferricyanide at a transport-controlled rate

downstream electrode:

$$Fe(CN)_6^{4-} - e^- \longrightarrow Fe(CN)_6^{3-}.$$

The experimental results are given in Table 1, and relate to a DCE geometry defined by $x_1 = 0.255$; $x_2 = 0.394$; $x_3 = 0.768$ cm. The corresponding theoretical collection efficiencies predicted in the absence of heterogeneous reactions in the gap using the theory given above are provided for reference. The excellent agreement between theory and experiment both corroborates our theoretical approach to this problem and verifies our method of measuring collection efficiencies. For comparison, the Matsuda/Braun analytical treatment of this problem, leading to the following expression for N [3, 4]:

Table 1. Collection efficiencies for the transport-controlled collection of ferrocyanide (at a Pt detector electrode) generated via the reduction of ferricyanide ions at the upstream electrode. Theoretical collection efficiencies in the absence of 'gap reactions' (k = 0) are shown for comparison. The DCE geometry is defined by: $x_1 = 0.255$; $x_2 = 0.394$; $x_3 = 0.768$ cm

V_f ($cm^3\ s^{-1}$)	*Collection efficiency*	
	Experimental	*Theoretical (k = 0)*
2.14×10^{-2}	0.351 (±0.006)	0.355
0.150	0.346 (±0.008)	0.352
2.47×10^{-3}	0.365 (±0.005)	0.362
2.24×10^{-3}	0.357 (±0.010)	0.363
2.72×10^{-3}	0.367 (±0.010)	0.362
1.32×10^{-2}	0.348 (±0.009)	0.356

$$N = 1 + \lambda^{2/3}[1 - F(\theta)] - (1 + \theta + \lambda)^{2/3} \times [1 - F((\theta/\lambda)(1 + \theta + \lambda))] - F(\theta/\lambda) \quad (26)$$

where

$$\theta = (x_2 - x_1)/x_1 \quad (27)$$

$$\lambda = (x_3 - x_2)/x_1 \quad (28)$$

and $F(\theta)$ is given by [21]:

$$F(\theta) = \frac{\sqrt{3}}{4\pi} \ln\left[\frac{(1 + \theta^{1/3})^3}{1 + \theta}\right] + \frac{3}{2\pi} \tan^{-1}\left[\frac{2\theta^{1/3} - 1}{\sqrt{3}}\right] + \frac{1}{4} \quad (29)$$

predicts a collection efficiency (independent of flow rate) of 0.350 for the DCE/cell geometry defined above. The similarity between this analytical theoretical result and those predicted numerically in Table 1 allows one to conclude that the DCE/cell geometry and flow rates employed in this particular example are within the bounds of the Lévêque approximation (*vide supra*) to within a few per cent. Thus a plot of I_{det} vs I_{gen} is predicted to be linear for a reversible couple and closely linear for an irreversible one [7, 14], the slope being given by the ratio of the transport-limited current at the two electrodes, $I_{gen,LIM}/I_{det,LIM}$. This fact justifies the choice of boundary condition at the generator electrode surface stipulated in the theoretical section. The effect of employing DCE geometries and flow rates which do not conform to the Lévêque approximation on the I_{det} vs I_{gen} relationship will be reported later [22].

We now turn to the use of the DCE for the evaluation of heterogeneous rate constants. Specifically, we consider the reaction between molecular bromine, generated amperometrically via the oxidation of bromide ions

$$Br^- - e^- \longrightarrow \tfrac{1}{2}Br_2$$

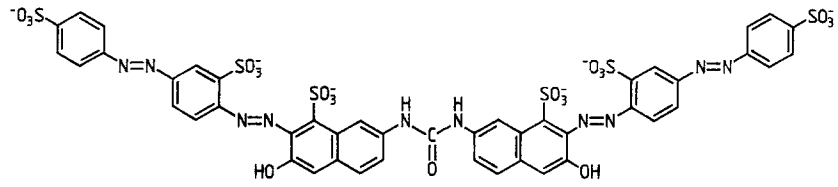

Fig. 8. Direct Red 80.

in 0.5 M sulphuric acid at the upstream electrode of a Pt DCE [23–28], and the dye Direct Red 80 irreversibly held on a cotton cloth located in the 'gap' of the DCE. The structure of Direct Red 80 is pictured in Fig. 8. The rate of the heterogeneous reaction was deduced by collecting bromine at a detector electrode positioned immediately downstream of the cloth, via transport-controlled reduction to bromide [23–28].

$$\tfrac{1}{2}Br_2 + e^- \longrightarrow Br^-$$

The homogeneous reaction of bromine with dyes of the general class to which Direct Red 80 belongs is well documented [29, 30], and preliminary experiments indicated that the dyed cloth could be slowly bleached by bromine water. We have previously shown that the dye is not released into aqueous acidic solutions from the cloth, and that there is no detectable reaction between bromine and the cotton substrate [13]. In the present work, bromine is generated from bromide ions, which are present in solution at the 1.0 mM level. Given the equilibrium constant [31]:

$$\frac{[Br_2]\,[Br^-]}{[Br_3^-]} \approx 6 \times 10^{-2}\ \text{mol dm}^{-3} \qquad (30)$$

in aqueous solution, we assume that the amount of Br_3^- present can be considered to be negligible under the conditions of the experiments. Measured collection efficiencies relating to this system for two DCE geometries and a range of flow rates are shown in Table 2. Also given are the collection efficiencies (calculated theoretically) that would be expected if Br_2 was transported to the detector electrode without loss through reaction. Diffusion coefficients for bromide and bromine of 1.82×10^{-5} and $9.4 \times 10^{-6}\ \text{cm}^2\ \text{s}^{-1}$ [28] were used in the calculation. It is evident that the experimental values are much lower than the theoretical $k = 0$ values, indicating that bromine is consumed by some reaction in the gap between the two electrodes before being detected downstream. Working curves (N vs k) for each of the flow rates and the relevant electrode geometry allowed the corresponding value of k to be deduced as listed in Table 2. The degree of agreement in the values of k determined using the two DCE geometries and a wide range of flow rates confirm the validity of the proposed DCE technique for the investigation of heterogeneous kinetics.

The range of rate constants which may be studied with the method is identified by considering Figs 4–6. For a channel flow cell 6 mm wide and 1 mm deep, an upstream electrode 2 mm long, a gap of 1–2 mm, a detector electrode in the range 2–8 mm and flow rates of 10^{-3}–1 $\text{cm}^3\ \text{s}^{-1}$ heterogeneous rate constants in the range 10^{-5}–10^{-1} cm s^{-1} may be measured. It is also apparent from Fig. 5 that the accuracy with which a particular rate constant may be determined is maximized with the appropriate tuning of flow rate and cell/DCE geometry. Given the wide range of rate constants which may be evaluated using the technique, DCE methodology should find application to a number of heterogeneous reaction systems.

Table 2. Experimental collection efficiencies for the transport-controlled collection of bromine (at a Pt detector electrode) generated via the oxidation of bromide ions at the upstream electrode, the gap consisting of cotton cloth dyed with Direct Red 80. The data relates to two DCE geometries. Theoretical collection efficiences in the absence of 'gap reactions' (k = 0) are shown for comparison. Measured collection efficiencies are interpreted in terms of the rate of reaction of bromine with Direct Red 80

DCE geometry			V_f *(cm³ s⁻¹)*	*Theoretical collection efficiency (k = 0)*	*Experimental collection efficiency*	10^4 k *(cm s⁻¹)*
x_1	x_2	x_3				
0.178	0.280	0.741	2.22×10^{-2}	0.434	0.380 (±0.006)	6.1 (+1.0; −0.8)
			1.64×10^{-2}	0.435	0.380 (±0.009)	5.7 (+1.4; −1.3)
			1.14×10^{-2}	0.436	0.380 (±0.010)	5.1 (+1.3; −1.1)
			2.42×10^{-2}	0.434	0.386 (±0.008)	5.5 (+1.1; −1.2)
			2.46×10^{-3}	0.443	0.351 (±0.005)	6.3 (±0.6)
			1.94×10^{-3}	0.445	0.350 (±0.001)	6.0 (±0.1)
			1.48×10^{-3}	0.447	0.343 (±0.006)	6.4 (+0.8; −0.6)
0.301	0.416	0.873	2.02×10^{-2}	0.386	0.345 (±0.007)	5.1 (+1.3; −1.1)
			0.198	0.382	0.354 (±0.008)	6.9 (+2.4; −2.1)
			2.64×10^{-3}	0.394	0.326 (±0.010)	5.1 (+1.3; −1.1)
			2.24×10^{-3}	0.395	0.327 (±0.011)	4.9 (+1.3; −1.2)
			1.70×10^{-3}	0.397	0.321 (±0.004)	5.2 (±0.5)

Acknowledgements

We thank the SERC and Ciba-Geigy Industrial Chemicals for a CASE award for P.R.U. and Unilever Research for support for A.J.B. We are grateful to Mr Roger Bowler for constructing the flow cell, Sally Barker for typing the manuscript and Mr David Kozlow for preparing the figures.

References

[1] A. N. Frumkin and L. I. Nekrasov, *Dokl. Akad. Nauk SSSR* **126** (1959) 115.
[2] H. Gerischer, I. Mattes and R. Braun, *J. Electroanal. Chem.* **10** (1965) 553.
[3] R. Braun, *J. Electroanal. Chem.* **19** (1968) 23.
[4] H. Matsuda, *J. Electroanal. Chem.* **16** (1968) 153.
[5] K. Aoki, K. Tokuda and H. Matsuda, *J. Electroanal. Chem.* **79** (1977) 49.
[6] W. J. Albery and M. L. Hitchman, 'Ring–Disc Electrodes', Clarendon Press, Oxford (1971).
[7] P. R. Unwin and R. G. Compton, *Compr. Chem., Kinet.* **29** in press.
[8] S. Moldoveanu and J. L. Anderson, *J. Electroanal. Chem.* **175** (1984) 67.
[9] J. L. Anderson and S. Moldoveanu, *J. Eectroanal. Chem.* **179** (1984) 107, 119.
[10] R. G. Compton, M. B. G. Pilkington and G. M. Stearn, *J. Chem. Soc. Faraday Trans. 1*, in press.
[11] R. G. Compton, B. A. Coles, G. M. Stearn and A. M. Waller, *J. Chem. Soc. Faraday Trans. 1*, in press.
[12] R. G. Compton, B. A. Coles and M. B. G. Pilkington, *J. Chem. Soc. Faraday Trans. 1*, in press.
[13] P. R. Unwin, A. J. Barwise and R. G. Compton, *J. Colloid Interface Sci.* in press.
[14] R. G. Compton and P. R. Unwin, *J. Electroanal. Chem.* **205** (1986) 1.
[15] B. A. Coles and R. G. Compton, *J. Electroanal. Chem.* **144** (1983) 87.
[16] K. Aoki, K. Tokuda and H. Matsuda, *J. Electroanal. Chem.* **217** (1987) 33.
[17] J. B. Flanagan and L. Marcoux, *J. Phys. Chem.* **78** (1974) 718.
[18] M. A. Lévêque, *Ann. Mines. Mem., Ser. 12* **13** (1928) 201.
[19] L. Lapidus and G. F. Pinder 'Numerical Solution of Partial Differential Equations in Science and Engineering', Wiley, NY (1982).
[20] V. G. Levich, 'Physicochemical Hydrodynamics', Prentice-Hall, Englewood Cliffs, NJ (1962).
[21] W. J. Albery and S. Bruckenstein, *Trans. Faraday Soc.* **62** (1966) 1920.
[22] R. G. Compton and G. M. Stearn, *J. Chem. Soc. Faraday Trans. 1*, in press.
[23] W. D. Cooper and R. Parsons, *Trans. Faraday Soc.* **66** (1970) 1698.
[24] W. J. Albery, M. L. Hitchman and J. Ulstrup, *Trans. Faraday Soc.* **64** (1968) 2831.
[25] W. J. Albery, M. L. Hitchman and J. Ulstrup, *Trans. Faraday Soc.* **65** (1969) 1101.
[26] W. J. Albery, A. H. Davis and A. J. Mason, *Faraday Discuss.* **56** (1974) 317.
[27] G. Faita, G. Fiori and T. Mussini, *Electrochim. Acta* **13** (1968) 1765.
[28] R. M. Machado and T. W. Chapman, *J. Electrochem. Soc.* **134** (1987) 387.
[29] H. A. Laitinen and K. W. Boyer, *Anal. Chem.* **44** (1972) 920.
[30] E. R. Wright, R. A. Smith and B. G. Messick, in 'Colorimetric Determination of Nonmetals (Chemical Analysis Vol. 8)' (edited by D. F. Boltz and J. A. Howell), Wiley, NY (1978) p. 44.
[31] R. O. Griffith, A. McKeown and A. G. Winn, *Trans. Faraday Soc.* **28** (1932) 101.